Two-Phase Flow Model of the Cathode of PEM Fuel Cells Using Interdigitated Flow Fields

Wensheng He, Jung S. Yi, and Trung Van Nguyen
Dept. of Chemical and Petroleum Engineering, University of Kansas, Lawrence, KS 66045

When interdigitated gas distributors are used in a PEM fuel cell, fluids entering the fuel cell are forced to flow through the electrodes porous layers. This characteristic increases transport rates of the reactants and products to and from the catalyst layers and reduces the amount of liquid water entrapped in the porous electrodes thereby minimizing electrode flooding. To investigate the effects of the gas and liquid water hydrodynamics on the performance of an air cathode of a PEM fuel cell employing an interdigitated gas distributor, a 2-D, two-phase, multicomponent transport model was developed. Darcy's law was used to describe the transport of the gas phase. The transport of liquid water through the porous electrode is driven by the shear force of gas flow and capillary force. An equation accounting for both forces was derived for the liquid phase transport in the porous gas electrode. Higher differential pressures between inlet and outlet channels yield higher electrode performance, because the oxygen transport rates are higher and liquid water removal is more effective. The electrode thickness needs to be optimized to get optimal performance because thinner electrode may reduce gas-flow rate and thicker electrode may increase the diffusion layer thickness. For a fixed-size electrode, more channels and shorter shoulder widths are preferred.

Introduction

The proton-exchange-membrane (PEM) fuel cell system is being seriously considered as an alternative power source for electric vehicles by virtual of its high-energy efficiency, pollution-free characteristic, and simplicity in design and operation. However, the performance of the PEM fuel cells needs to be further improved to increase their cost-effectiveness so that they can compete against the traditional combustion engines. Of the performance controlling components in a PEM fuel cell, the cathode is recognized to be one of the most influential components due to the slow kinetic rate of the oxygen reduction reaction. The performance of the cathode also depends highly on the oxygen transport rate that is strongly affected by the presence of liquid water. Cathode flooding caused by excessive liquid water in the cathode is generally recognized as the primary reason for poor cell performance.

Recently, the interdigitated flow field design was proposed to solve the cathode-flooding problem (Nguyen, 1996). Experimental results have shown that this new flow field design leads to a performance improvement ranging from 50% to over 100% (Wood et al., 1998). The improvement was attributed to the fact that the dead-end flow channels converted the transport of the reactants and products in the porous electrode from a diffusion mechanism to a forced convection mechanism. More importantly, the shear force exerted by the gas flow helps to remove most of the liquid water that is entrapped in the porous electrode, thereby minimizing electrode flooding.

Several modeling attempts have been made to help understand the effects of the new flow field design (Yi and Nguyen, 1996, 1998, 1999; Yi, 1998, and Nguyen, 1999). Yi and Nguyen (1996) presented the first model of the hydrodynamics of a reactant gas in a porous electrode of a PEM fuel cell with the interdigitated flow fields. This model was then extended to multicomponent to account for the effects of inert species such as nitrogen and water vapor (Yi and Nguyen, 1999). However, these previously published models (including most models of PEM fuel cells using conventional flow field (Gurau et al., 1998)) are all single-phase models. They have assumed that water existed only in vapor form in the porous elec-

Correspondence concerning this article should be addressed to T. Van Nguyen.

trodes and, therefore, cannot account for the effects of active catalyst surface coverage and pore plugging by liquid water. Obviously, the performance predicted by these models would deviate from the actual performance of PEM fuel cells operated at high current densities where the cell performance is greatly affected by cathode flooding. To account for the effects of cathode flooding, a two-phase flow model is necessary. Yi and Nguyen (1998), Yi (1998), and Nguyen (1999) included the effects of liquid water in their latter models by including the interfacial mass transport between the two phases by evaporation and condensation and the transport of liquid water. These two-phase models used the mass-based conservation equations, which are inconvenient to use especially in the interfacial mass transport equation and current density calculations where molar concentrations are used. Furthermore, the transport of liquid water in the porous electrode that is induced by capillary force and gas flow-driven shear force was treated by semi-heuristic equations.

In this article, a two-phase, two-dimensional (2-D), steady-state, isothermal model is developed to investigate the effects of liquid water and its transport on the performance of the cathodes of PEM fuel cells employing the interdigitated flow fields. All equations are molar-based. A different interfacial mass transport equation is used to account for the evaporation and condensation of water vapor, and a new equation of motion for the liquid water is derived. The physical significance of these equations is explained in this article. The model is then used to look at the effects of various electrode and flow field design parameters on the performance of a cathode of a PEM fuel cell using an interdigitated flow field, and the results of these case studies are presented in the latter parts of this article.

Model Description and Assumptions

The modeled region consists of the porous layer in contact with an interdigitated gas distributor which has an inlet channel, a shoulder, and an outlet channel to allow gas to flow through the electrode (see Figure 1). In a typical operation, dry air is supplied to the inlet channel as the oxygen source. Water is generated at the membrane and electrode interface by the oxygen reduction reaction and net water migration from the anode. It is assumed here that water is generated as liquid, because typical operating temperatures of PEM fuel cells are below 100°C. Depending on the local partial pressure of water and its saturation vapor pressure at the operating temperature, liquid water can evaporate or water vapor can condense. If the water generation rate exceeds its removal rate in the form of vapor, liquid water is present in the electrode. The presence of liquid water contributes to electrode flooding by blocking active sites on the catalysts and reducing the gas volume in the porous electrode. This leads

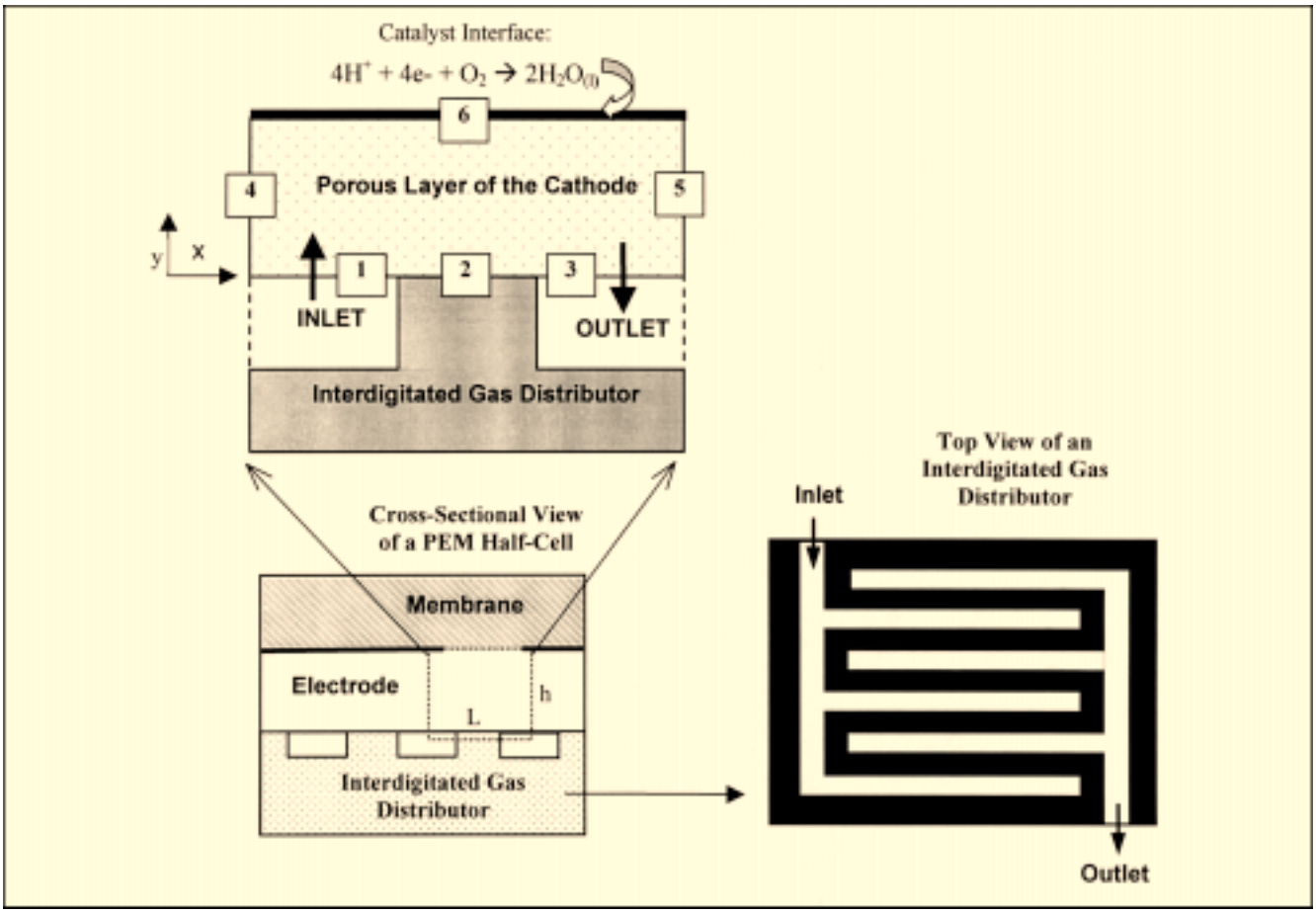

Figure 1. Modeled region

to a smaller active area available for reaction and reduced area and volume for oxygen gas transport.

In this study, the electrode layer is treated as a homogeneous porous medium with uniform morphological properties such as porosity, tortuosity, and permeability. The gas and liquid phases within the electrode exist as continuous phases, so that Darcy's law applies. The gas mixtures are considered to be perfect gases. The catalyst layer is treated as an ultrathin layer; thus the transport of the reactants within this layer can be neglected. Other assumptions will be discussed as the model equations are presented.

Governing Equations

The continuity equation for the gas phase is

$$0 = \nabla\cdot(C^g \upsilon^g) + r_w \tag{1}$$

where C^g is the total molar concentration of the gas phase, and ν^g is the superficial velocity of the gas phase which represents the volumetric flow rate per unit cross-sectional area of both solid and fluid. The term r_w represents the interfacial mass-transfer rate of water by condensation or vaporization. From ideal gas law

$$C^g = \frac{P}{RT} \tag{1a}$$

where P and T are the pressure (atm) and temperature (°C) of the gas phase, respectively.

The interfacial mass-transfer rate of water between the gas and liquid phases r_w is

$$r_w = k_c \frac{\epsilon^g y_w}{RT}\left(y_w P - P_w^{\text{sat}}\right) q + k_\nu \frac{\epsilon_0 s \rho_w}{M_w}\left(y_w P - P_w^{\text{sat}}\right)(1-q) \tag{2}$$

where q is a switching function that was selected such that it is one when the water partial pressure is greater than the water saturation pressure and zero otherwise. In this study, a switching function defined as following is used

$$q = \frac{1 + |\left(y_w P - P_w^{\text{sat}}\right)|/\left(y_w P - P_w^{\text{sat}}\right)}{2} \tag{3}$$

The first term in the righthand side of Eq. 2 represents the condensation rate while the second term represents the evaporation rate. Equation 2 is basically assuming that the interfacial mass-transfer rate is proportional to the amount of the reactant in the porous media and the driving force, the difference between water partial pressure and its saturation pressure. In Eq. 2, k_c and k_υ are the rate constants for condensation (s^{-1}) and vaporization, (cm/atm − s) respectively, y_w is the mol fraction of water vapor is gas phase, P is the total pressure of the gas phase, P_w^{sat} is the saturation pressure of water at operating temperature, R and T are gas constant and operating temperature (°C), respectively, M_w is the molecular weight (g/mol) of water, ϵ_o is the dry porosity of the electrode, s is the saturation level of liquid water, defined as the fraction of the void volume occupied by liquid phase, ϵ^g is the gas porosity, defined as $\epsilon^g = \epsilon_0(1-s)$, and ρ_w is the density (g/cm^3) of liquid water.

There are three components in the gas phase, N_2, O_2, and H_2O. Therefore, two independent component mass balance equations are needed. For O_2.

$$\nabla\left(C^g \upsilon^g y_o - C^g D_O^e \nabla y_O\right) = 0 \tag{4}$$

and for H_2O vapor

$$\nabla\left(C^g \upsilon^g y_w - C^g D_w^e \nabla y_w\right) + r_w = 0 \tag{5}$$

where D_i^e is the effective diffusivity of component i in the porous electrode. D_i^e is related to its binary diffusivity by the following equation (Bear and Buchlin, 1991)

$$D_i^e = D_i\left(\epsilon^g\right)^{1.5} \tag{6}$$

The pressure dependence of D_i and the effect of dispersion are neglected in this model. The temperature dependence of the binary diffusion coefficient is obtained from Bird et al. (1960)

$$D_i = D_{i,r}\left(\frac{T}{T_r}\right)^b \tag{6a}$$

The gas-phase velocity (cm/s) ν^g is estimated by Darcy's law, neglecting the effect of gravity

$$\nu^g = -\frac{K_o(1-s)}{\mu}\nabla P \tag{7}$$

where K_o is the gas permeability of a dry electrode, and μ is the viscosity (g/cm − s) of the gas mixture. The term $(1-s)$ is added to account for the changes in the gas porosity because of the presence of the liquid phase (Adler, 1992; Bear and Buchlin, 1991).

The mass balance for liquid water is

$$0 = \nabla\cdot\left(\frac{\epsilon_o s \rho_w}{M_w}\nu^l\right) - r_w \tag{8}$$

where ν^l is the interstitial velocity of liquid water in the porous electrode.

For liquid water phase, the momentum conservation also follows Darcy's equation, neglecting gravitational effect

$$\nu^l = \frac{K^l}{\mu^l}\nabla p^l \tag{9a}$$

where K^l, μ^l and p^l are the permeability, viscosity, and pressure of the liquid phase, respectively.

From the definition of capillary pressure, p^c

$$p^l = P - p^c \tag{9b}$$

where P is the pressure of gas phase, Eqs. 9a and 9b can be

combined to yield

$$\nu^l = \frac{K^l}{\mu^l}\nabla P + \frac{K^l}{\mu^l}\nabla p^c = -\frac{K^l}{\mu^l}\frac{\mu^g}{K_o(1-s)}\frac{K_o(1-s)}{\mu^g}\nabla P + \frac{K^l}{\mu^l}\frac{dp^c}{ds}\nabla s \quad (9c)$$

If we define

$$f = \frac{K^l}{\mu^l}\frac{\mu^g}{K_o(1-s)} = \frac{K^l}{\mu^l}\frac{\mu^g}{K^g}$$

as the interfacial drag coefficient and

$$D_c = -\frac{K^l}{\mu^l}\frac{dp^c}{ds}$$

as a capillary diffusion coefficient and substitute Eq. 7 into Eq. 9c, the equation of motion for liquid water becomes

$$\nu^l = f\nu^g - D_c\nabla s \quad (10)$$

Note that D_c has the units of cm^2/s, which are the same as those of the normal diffusivity. A similar definition of D_c is used in literature, such as Wang and Cheng (1997). Equation 10 clearly shows that, within the porous electrode, the transport of liquid water is driven by two mechanisms: capillary force (driven by saturation gradient) and interfacial shear force (exerted by gas flow). Practically, K^l and dp^c/ds can be some complex functions of liquid saturation. However, if the variation of s is small (about 0.1 for our base case), it is a fairly good assumption to assume that f and D_c are constant. For simplicity, this assumption is used in this study.

Modeling two-phase flow in a porous medium is a very challenging problem because of the extreme complexity of the system. Very little rigorous theoretical analysis has been attempted to account for the interfacial drag forces (see Kaviany (1995)), which are very important in this case. The use of Eq. 10, which is given in terms of measurable quantities (∇P and ∇s), gives us a clear picture of the two mechanisms involved in liquid water transport in the porous electrode. Its use also greatly simplifies the numerical solution procedures of this model.

Boundary Conditions

At the inlet, $y = 0$ and $0 \le x < \mathrm{L1}$ (boundary 1 in Figure 1), where the reactant gases are fed to the electrode, the pressure is set equal to the inlet pressure, and the flux of each gas species from the channel to the electrode is conserved

$$P = P_{\text{in}} \quad \text{and} \quad -D_i^e\frac{\partial y_i}{\partial y}\bigg|_{y=o+} + y_i\nu_y^g = y_i^{\text{in}}\nu_y^g \quad (11)$$

Note that Neumann-type and not Dirichlet-type boundary condition is used for the gas species, because in regions close to the symmetry line (boundary 4) convective flow is very low and back diffusion becomes significant (that is, $y_i|_{y=o+} \neq y_i^{\text{in}}$). Use of Dirichlet boundary condition here led to erroneous results. For the cathode side of the electrode where either dry or partially hydrated air is used, the flux of liquid water at this boundary is set equal to zero

$$\frac{\epsilon s\rho_w}{M_w}\nu_y^l = 0 \quad (12)$$

At the interface in contact with the shoulder of the gas distributor, $y = 0$ and $L1 \le x \le L2$ (boundary 2), where all fluxes in the y-direction are assumed to be zero, the following equations are used

$$\frac{\partial P}{\partial y} = 0, \quad \frac{\partial y_o}{\partial y} = 0, \quad \frac{\partial y_w}{\partial y} = 0, \quad \frac{\partial s}{\partial y} = 0 \quad (13)$$

At the outlet interface, $y = 0$ and $L2 < x \le L$ (boundary 3), the outlet pressure is specified and changes in the mass fractions and saturation density of liquid water are assumed to stop

$$P = P^{out}, \quad \frac{\partial y_o}{\partial y} = 0, \quad \frac{\partial y_w}{\partial y} = 0, \quad \frac{\partial s}{\partial y} = 0 \quad (14)$$

At the boundaries where $x = 0$ or L and $0 < y < h$ (boundaries 4 or 5), symmetry conditions are used because $x = 0$ and L are the center points of the flow channels

$$\frac{\partial P}{\partial x} = 0, \quad \frac{\partial y_o}{\partial x} = 0, \quad \frac{\partial y_w}{\partial x} = 0, \quad \frac{\partial s}{\partial x} = 0 \quad (15)$$

At the electrode/membrane interface ($0 < x < L$, and $y = h$, boundary 6), the y-directional superficial gas velocity, $v_y^g|_{y=h}$ is assumed to be zero. Therefore, the following expression for the pressure is applied at the interface

$$\frac{\partial P}{\partial y} = 0 \quad (16)$$

However, at this interface, oxygen reacts with protons and electrons to form water

$$2H^+ + \frac{1}{2}O_2 + 2e^- \rightarrow H_2O_{(l)} \quad (17)$$

Also, water is transported from anode side of the membrane to the cathode by electroosmosis. By these two mechanisms, water is introduced into the electrode from this interface as liquid water. Therefore, the mass fluxes of oxygen and liquid water can be defined as a function of the local current density I, (A/cm^2) as follows

$$-C^gD_o^e\frac{\partial y_o}{\partial y}\bigg|_{y=h} = \frac{I}{4F} \quad (18)$$

$$\frac{\epsilon s\rho_w}{M_w}\nu^l\bigg|_{y=h} = -\left(\frac{1}{2}+\alpha\right)\frac{I}{F} \quad (19)$$

As given in Eq. 19, the liquid water flux at the electrode/membrane interface arises from two sources, the oxygen reduction reaction and electro-osmosis. The parameter α represents the net water transport coefficient in the membrane and is assumed to be constant. Next, the mass flux of water vapor at the reaction surface is zero

$$- C^g D_w^e \frac{\partial y_w}{\partial y}\bigg|_{y=h} = 0 \tag{20}$$

The Tafel equation is used to describe the local current density along the catalyst layer as a function of the oxygen concentration at the electrode/membrane interface and the electrode overpotential η which is a set parameter in the model

$$I = I_o \frac{\epsilon^g}{\epsilon_o} \frac{C^g y_o}{C_{o,\text{ref}}} \exp\left(\frac{kF}{RT}\eta\right) \tag{21}$$

where I_o is the exchange current density (A/cm^2), $C_{o,\text{ref}}$ is the oxygen reference concentration (mol/cm^3) such as 1 atm, 25°C and k is the transfer coefficient for the oxygen reaction. When liquid water is present at the reaction interface, it covers the available reaction sites and hinders the oxygen transport to the reaction site. The effect of liquid water on the surface availability of the reaction site is accounted for in Tafel equation by the term ϵ^g/ϵ_o.

The governing equations along with boundary conditions are fully discretized using the finite difference method, yielding a system of algebraic equations. The primary independent variables are the total pressure of gas, oxygen mol fraction, water vapor mol fraction, and liquid saturation. This algebraic system of equations is solved using a banded solver given by Nguyen and White (1987). Once the partial pressures of oxygen along the reaction interface are known, the local current densities along the interface are calculated from Eq. 21, and the average current density is estimated by integrating the current densities generated along the x-direction suing Simpson's method.

Results and Discussion

When an interdigitated gas distributor is used with an air cathode, oxygen and water are transported to and from the inner layer of the electrode by both diffusion and convection that is induced by the pressure drop created between the noninterconnected inlet and outlet channels of the interdigitated gas distributor. This through-the-electrode convective flow reduces the gas diffusion distance to and from the catalyst layer, and by having gas flown over the shoulders of the gas distributor, the electrode active area over the shoulder is better utilized (Yi and Nguyen, 1995; West and Fuller, 1996). Also, the shear force of the gas stream helps remove the liquid water that is entrapped in the electrode layer thereby reducing the electrode flooding problems. These benefits help extend the cell operable regime to higher current densities and consequently higher power densities. Previous results from a gas-phase multicomponent model of the interdigitated gas distributor have shown that the stagnant layer was significantly reduced when the gas was forced to flow through the diffusion layer (Yi and Nguyen, 1995, 1996). However, to obey the assumption of single-phase (vapor) water, the previous study investigated only low current density performance where the water vapor pressure stays below the saturated vapor pressure of water. By extending this model to a two-phase system, the cathode performance at high current densities, where liquid water is more likely to be present, can now be investigated. Note that when the liquid saturation s, goes to zero (that is, at low current densities) this model becomes a single-phase model. The two-phase transport model can be used to study the effects of gas and liquid flow characteristics and various operating and design parameters, such as the pressure drop across the channels, electrode thickness, and shoulder width, on the performance of a cathode in contact with an interdigitated flow field.

The remaining sections of this article discuss some results of this study. For comparison purpose, a base case consisting of an air electrode with a porosity of 0.3 and a height of 0.025 cm in contact with a gas distributor, which has 0.1 cm inlet and outlet channel width and 0.1 cm shoulder width, is chosen. These values represent actual dimensions used in our fuel cells with size ranging from 4 cm^2 to 120 cm^2 and power from 4 W to 120 W. A pressure drop of 0.007 atm is applied between the inlet and outlet channels. This pressure drop value was measured experimentally for an air stoichiometric flow rate of 1.3. For the cathode overpotential 0.50 V is used. Other conditions and parameters used in the study are shown in Table 1 along with the references for various parameters used in the model.

Table 1. Values for Parameters Used in the Base Case

Inlet channel width (Half)*	0.05 cm
Shoulder width*	0.10 cm
Outlet channel width (Half)*	0.05 cm
Electrode height*	0.025 cm
Gas permeability of the electrode (κ)**	1.2×10^{-8} cm^2
Dry porosity of the electrode (ϵ_0)	0.3
Inlet mol fraction of oxygen	0.21
Inlet mol fraction of water	0.00
Inlet mol fraction of nitrogen	0.79
Inlet channel pressure	1.007 atm
Outlet channel pressure	1.0 atm
Temperature	60°C
Gas viscosity (μ) at 60°C†	2.03×10^{-4} g/cm − s
D_o (at T_r)††	0.1775 cm^2/s (0°C)
D_w (at T_r)††	0.256 cm^2/s (at 34°C)
Capillary diffusion coefficient of liquid water (D_c)	1.0×10^{-4} cm^2/s
Interfacial drag coefficient ($f \sim \mu_g \kappa_l/\mu_l \kappa_g$)	0.005
Condensation rate constant (k_c)‡	100/s
Vaporization rate constant (k_v)‡	100/atm·s
Exchange current density at 60°C (I_0)‡‡	1×10^{-2} A/cm^2
Transfer coefficient of oxygen reduction reaction (k)‡‡	0.5
Overpotential (η)	0.50 V
Net water transport coefficient of the membrane (α)§	0.5

*Actual size.
**Estimated from experiments when dry porosity is 0.3.
†Bird et al. (1960).
††Cussler (1984).
‡Chosen such that both rates are fast enough.
‡‡Paik et al. (1989), with I_o adjusted for temperature and active surface area.
§Yi, (1998).

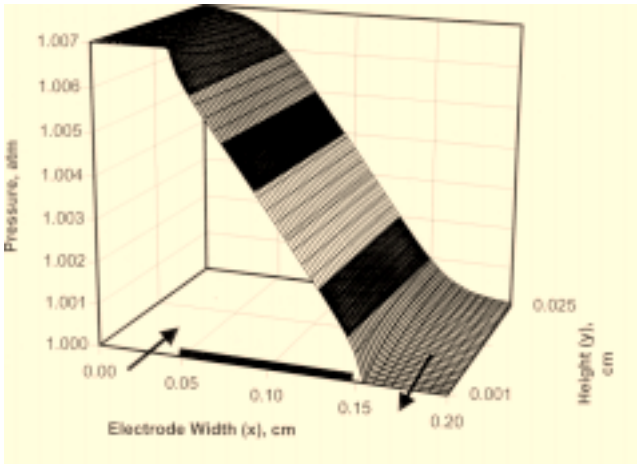

Figure 2. Pressure distribution in the electrode for the base case.

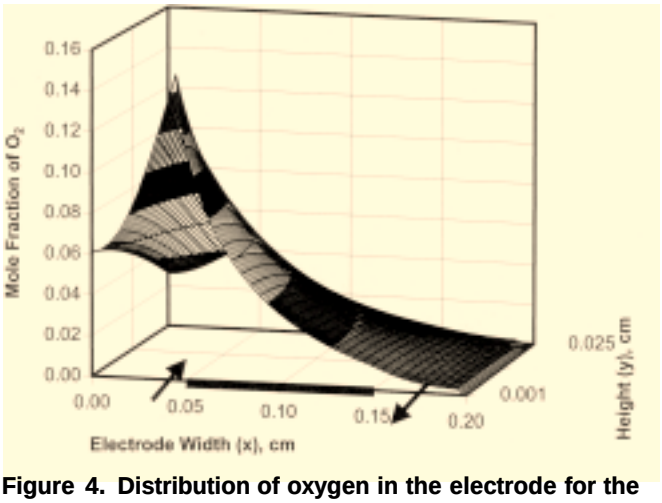

Figure 4. Distribution of oxygen in the electrode for the base case.

Base Case

The results for the base case are given in Figures 2 to 7. Figure 2 shows the pressure distribution within the electrode. Pressure drops along the electrode height are small except near the inlet/shoulder and outlet/shoulder corners where both the *x*-direction and *y*-direction velocities (see Figure 3) are highest. Most of the pressure drops are located in the x-direction between the inlet and outlet channels.

The y-direction velocity is smaller in the region near the reaction interface than the x-direction velocity because the mass flux in the y-direction created by the electrode reaction is much smaller. The velocities profiles observed in the porous layer can be explained as follows. At the inlet, the y-direction velocity is high, and since only a small amount of gas goes into the electrode/membrane interface to support the reaction, it quickly decreases and transfers its momentum to the x-direction velocity. The same thing occurs at the outlet with x-direction velocity decreasing and transferring the momentum to y-direction velocity, which now goes in the opposite direction. These velocities peak near the inlet/shoulder and outlet/shoulder corners because they constitute the shortest distance between the channels.

The mole fraction profiles of oxygen, water vapor and saturation density of liquid water are given in Figures 4, 5 and 6. Above the inlet ($0 < x < 0.05$), with more oxygen flowing into the electrode near the inlet/shoulder corner, as shown in Figure 3, the oxygen fraction is highest at this corner. From there, the oxygen concentration decreases as oxygen moves from the inlet toward the electrode/membrane interface, where it is consumed as shown in Figure 4. The oxygen fraction within the electrode layer continues to decrease along the x-direction as oxygen is continuously consumed along the membrane/electrode interface. Water is generated as a liquid at the electrode/membrane interface and dispersed by capillary diffusion and convection by the shear force of gas flow, as shown in Figure 6. The generated liquid water is

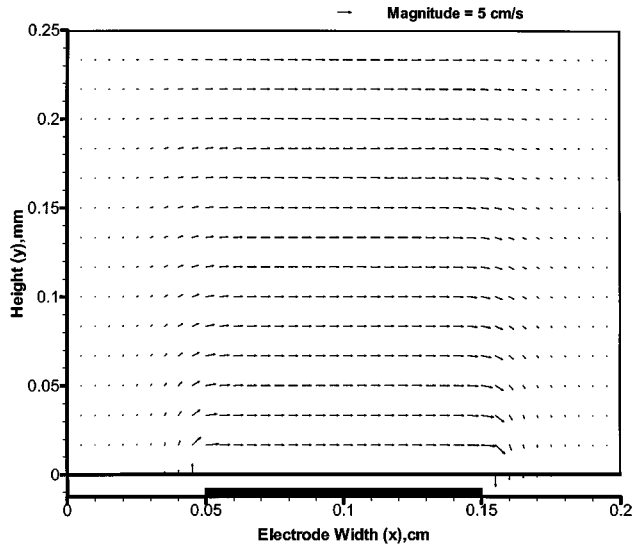

Figure 3. Vector plot of the gas velocity in the electrode for the base case.

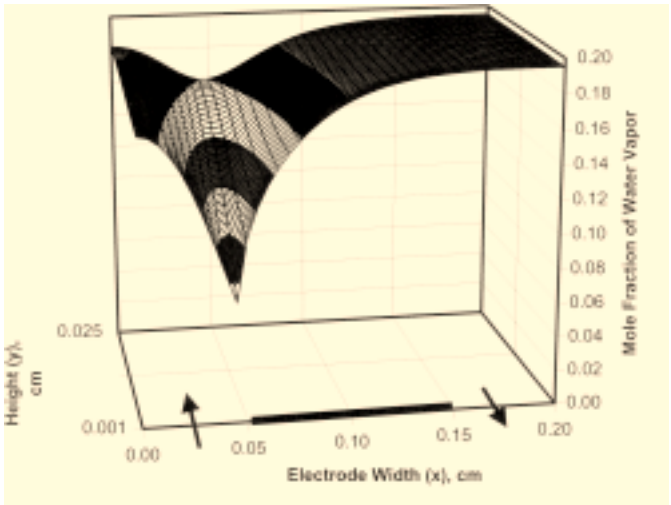

Figure 5. Distribution of water vapor in the electrode of the base case.

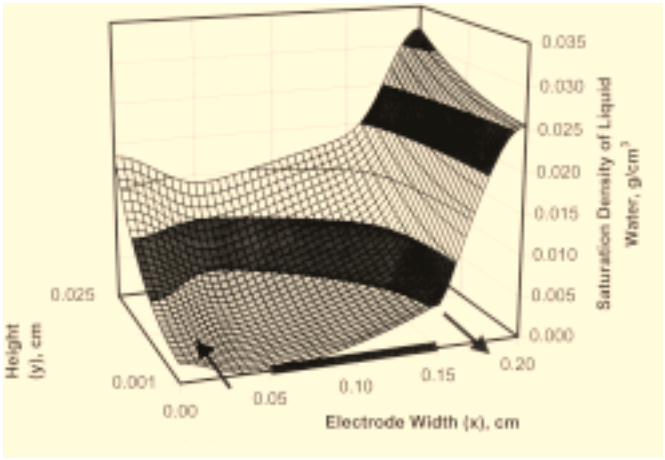

Figure 6. Distribution of liquid water in the electrode for the base case.

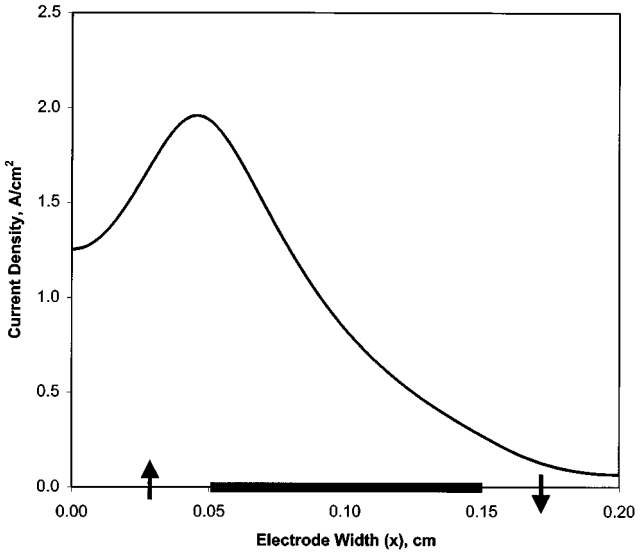

Figure 7. Current density profile along the electrode width for the base case.

carried along the electrode and toward the outlet by the x-direction velocity and then out of the electrode by both the y-direction velocity and capillary diffusion. The local liquid water maximum observed at the corner of the electrode atop the outlet is attributed to the fact that there is little x-direction and y-direction convective flow at this corner. At this location, capillary diffusion is the only mechanism for liquid water removal.

Liquid water is also removed from the electrode by another mechanism. It can vaporize and be transported out in the form of water vapor by diffusion and as part of the convective gas flow. Figure 5 shows the water vapor profile in the electrode from the inlet to the outlet. In the region above the inlet channel, the concentration of water vapor in the gas phase increases as the center of the inlet ($x = 0$) is approached. This is attributed to the higher back diffusion rate of water vapor and capillary transport rate of liquid water from the reaction interface relative to the opposing gas incoming flow rate, which is smallest near the center of the inlet. Characteristics of this region approach that of a conventional gas distributor design, where gas and liquid are transported to and from the reaction interface solely by diffusion and capillary transport. After the inlet/shoulder corner, the water vapor fraction increases continuously along he shoulder region to the outlet as water is generated along the reaction interface. Note that the gas phase is essentially saturated with water vapor by the time it reaches the outlet. A significant amount of liquid water generated at the reaction interface is removed from the electrode in the form of water-vapor-saturated gas stream when air is used. The remaining amount of liquid water is carried out by he combination of capillary force and shear force of gas flow.

The additional amount of water vapor in the gas phase explains the higher magnitudes of the velocities for both directions at the outlet than those at the inlet (see Figure 3) and the rapid decrease in oxygen concentration toward the outlet (see Figure 4). The shape of the mol fraction profile of oxygen along the reaction interface explains the current density profile along this interface and the peak current density above the inlet/shoulder corner, as shown in Figure 7. The air cathode average current density for the base case is calculated to be 0.91 A/cm^2.

Validation of the Model with Experimental Data

To validate this two-phase model, the model results are compared to a set of experimental data collected on a 9-cm^2 cell at the same conditions as the base case except that the air-flow rate was at 2.0 A/cm^2-equivalent O_2. The physical parameters of the gas-flow fields are exactly as those shown in the base case. Nafion 115 (thickness $\cong$ 125 μm) was used as the membrane. The catalyst layers are about 60–70 μm each. To simulate the actual air-flow rate, an inlet pressure of 1.0133 atm is used. The open circuit potential of the cell is 1.0V. The other parameters are the same as the base case.

To account for the ohmic loss of the cathode catalyst layer, a conductivity of 0.53 S/cm is used (Bernardi and Verbrugge, 1992). The reported ionic conductivity of a well-hydrated Nafion membrane at about 60°C ranges from 0.07 to 0.144 S/cm (Sone et al., 1996; Nouel and Fedkiw, 1998). The conductivity of Nafion used in this study is 0.11S/cm, which is the average of the two reported values. There is another source of cell voltage loss in PEM fuel cell operation—the anode overpotential, which is usually ignored by most of the previous PEM fuel cell models. It is true that the cell performance is not likely to be limited by the H_2 oxidation kinetics, because it is very fast compared to that of oxygen reduction at the cathode. However, this does not necessarily mean that there is no overpotential loss in the anode. The reported anode overpotential for PEM fuel cells range from 40 to 80 mV at the current density of a A/cm^2, depending on the configuration of the anode (Watanabe et al., 1998; Wang and Savinell, 1992). To account for anode overpotential loss in this study, an anode overpotential of 52 mV at current density of 1 A/cm^2 is used, and a linear relationship between anode overpotential and current density is assumed. The model results and the experimental data are presented in Figure 8.

It is clearly shown in Figure 8 that, after the correction for ohmic loss of the membrane and catalyst layers and anode overpotential loss, the model results agree very well with the

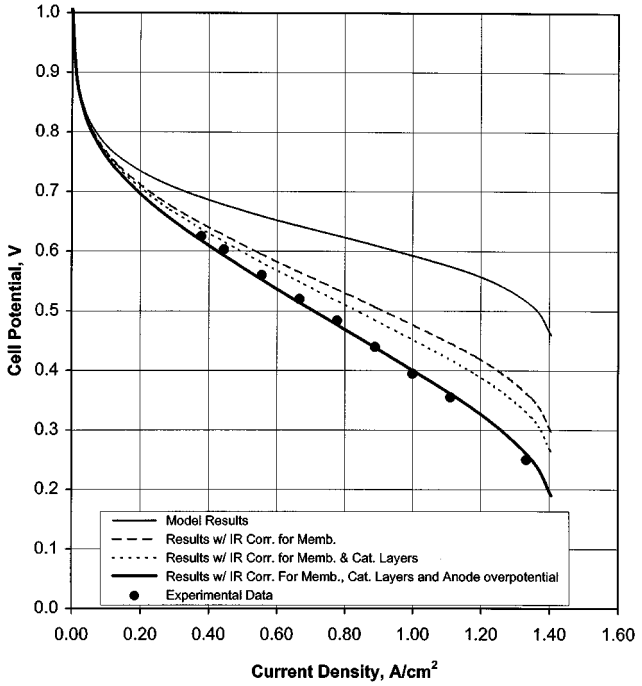

Figure 8. Comparison of experimental data with model results.

experimental data. One might note that there is no data in the current density range from 0 to about 0.35 A/cm^2. This is because the minimum current that can be controlled by the electronic load used in our fuel cell test station is about 3 A, or 0.33 A/cm^2 for a 9-cm^2 cell. Figure 8 also clearly breaks down the sources for the cell voltage losses. In the whole operating range, losses due to cathode overpotential and O_2/H_2O transport resistance at high current densities are the dominant sources. The ohmic loss by the membrane is the second largest contributor to the cell voltage loss. These observations are consistent with those reported by Bernardi and Verbrugge (1992). Finally, these results tell us that, to improve the PEM fuel cell performance, the efficiency of cathode catalyst, the transport of oxygen and water, and the ionic conductivity of the membrane need to be optimized.

Effect of Differential Pressure

Figure 9 shows the effects of pressure drop between the inlet and outlet channels of an interdigitated gas distributor on the performance of the cathode. In this study, outlet pressure is maintained at 1 abs atm and the inlet pressure is varied to create the differential pressures. As the differential pressure increases, the air-flow rate through the electrode increases resulting in a thinner diffusion (stagnant) layer for faster transport of oxygen to the reaction sites, higher oxygen concentrations throughout the electrode, and, consequently, higher current densities at a fixed overpotential. Note that at low current densities where the performance is kinetically controlled, the improvements in the performance caused by higher differential pressure and gas-flow rates are small as expected. Larger pressure drop extends the mass-transport-limiting region to higher current densities because of the enhanced oxygen transport and a higher removal rate of liquid water from the electrode. Note that the pressure drop required to generate high gas-flow rate is very small due to the high permeability of the electrode and short width of the shoulder.

Figure 10 shows the current density distribution along the electrode at three different differential pressures. One can see that higher differential pressures result in higher current densities at every point along the electrode/membrane reaction interface from the inlet to the outlet. Note that the in-

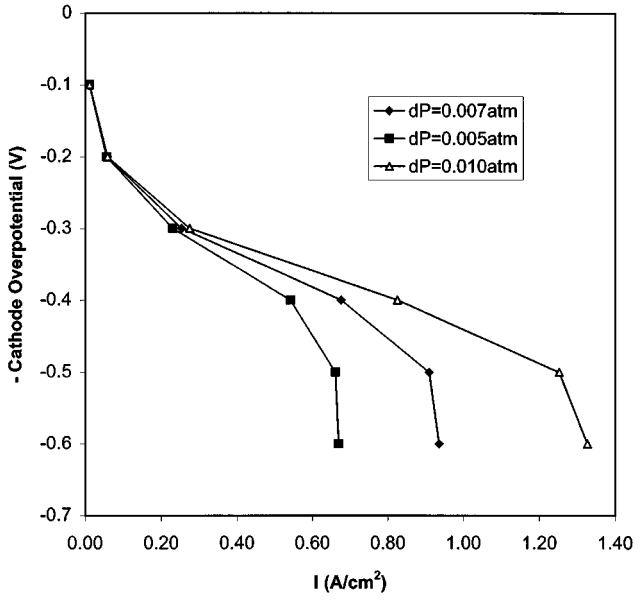

Figure 9. Effect of differential pressure on the performance of the cathode.

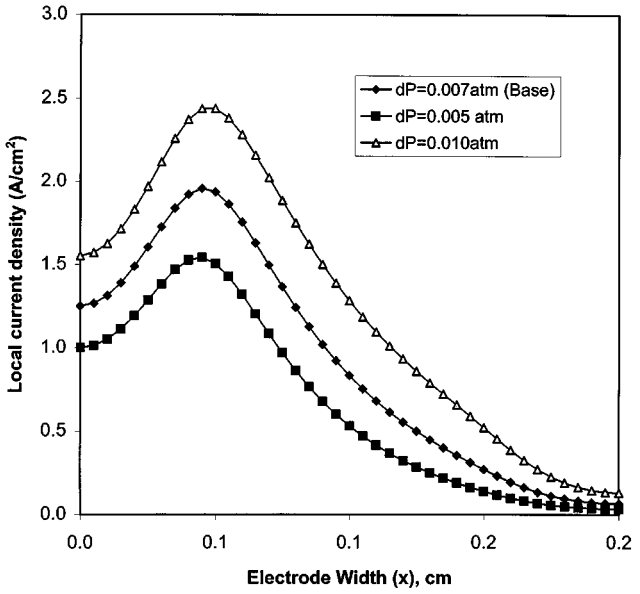

Figure 10. Effect of differential pressure on the local current density profiles along the electrode width (at an overpotential of 0.5 V).

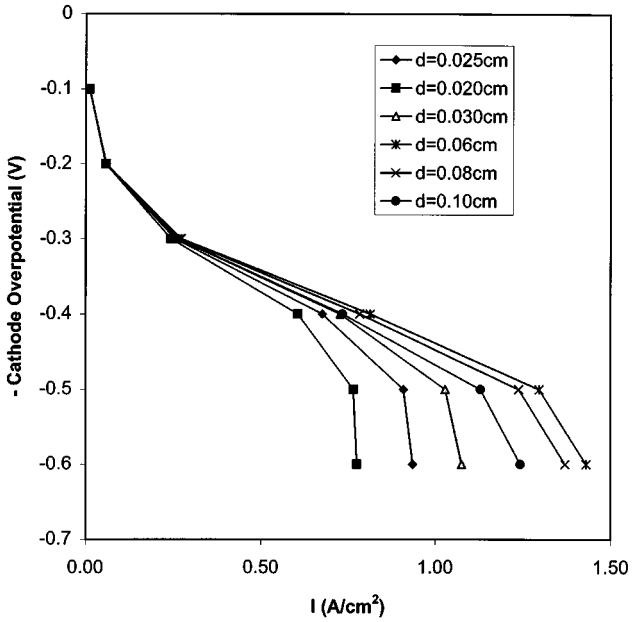

Figure 11. Effect of electrode thickness on the performance of the cathode.

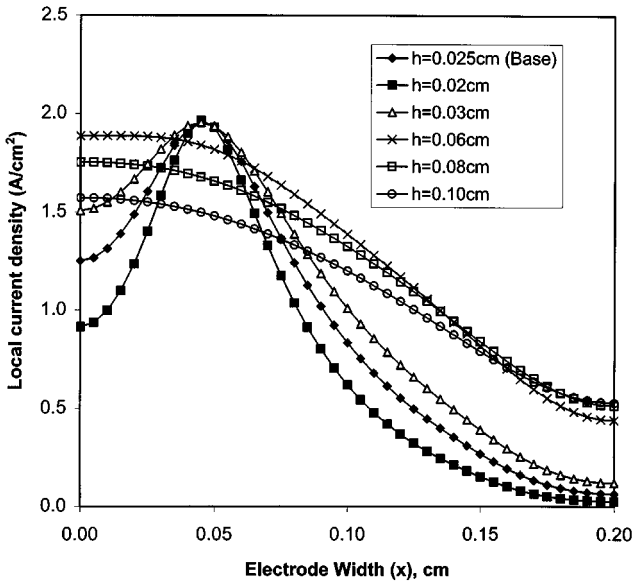

Figure 12. Effect of electrode thickness on the current density profiles along the electrode width (at an overpotential of 0.5 V).

crease in the current density is greater along the section near the inlet of electrode. This is to be expected because of higher oxygen concentration in this region. From the results shown in Figure 10, one would expect the current density profile to become flatter and the average current density to be higher with higher air-flow rate. However, we will show later that high gas-flow rate alone is not the key to improving the performance of an air cathode with an interdigitated gas distributor. Electrode design parameters play a significant role as well.

Effect of Electrode Thickness

All the following simulations are performed at a fixed differential pressure of 0.007 atm (700 Pa). The effects of the electrode thickness on the current density are investigated, and the results are presented in Figures 11 and 12. Other conditions are the same as the base case. Figure 11 shows that when the electrode thickness is between 0.02 cm and 0.06 cm, the average current density increases as the electrode thickness increases. However, as the electrode thickness increases beyond 0.06 cm, the performance decreases. Increasing the electrode thickness is equivalent to increasing the diameter of a pipe in a fluid flow system, thereby decreasing flow resistance, which translates to higher gas-flow rate for the same differential pressure. As a result of enhanced oxygen transport and liquid water removal rate, the average current density increases as the electrode thickness increases from 0.02 to 0.06 cm. However, beyond 0.06 cm, higher gas-flow rate does not result in a thinner diffusion layer because most of the gas now takes the shortest route through the electrode (between the inlet/shoulder and outlet/shoulder corners) resulting in a thicker diffusion layer and, consequently, a lower average current density. Therefore, for an electrode thickness greater than 0.06 cm, the average current density decreases, as shown in the Figure 11. Figure 12 shows the local current density distribution along the electrode interface for the six electrode thickness cases. Note that the gas bypassing effect becomes more severe as the electrode thickness increases further. From these results, it is clear that there is an optimum electrode thickness, and its value depends on the electrode morphology and the gas distributor design parameters.

It is important to point out that the effect of ohmic voltage loss due to the electronic conductivity of the electrode is not considered here. Even though it is not expected to be significant within the range of electrode thickness considered, the effect of ohmic voltage loss should not be ignored in the optimization of the cell performance.

Effect of Number of Channels

For a fixed-size electrode, the number of channels is an important design factor of the gas distributor. In this section, the effect of the shoulder width, which corresponds to the number of channels in the gas distributor when the ratio between channel and shoulder width is fixed at 1:1, is studied. For a fixed length of the modeling region (0.4 cm), three different designs are evaluated (see Figures 13 and 14). Based on the symmetry nature of the shoulder and channel widths, a repeating unit consisting of a half width of inlet channel, a full width of shoulder, and a half width of outlet channel is used to simulate each design. The same differential pressure as in the base case is applied to all three cases. As shown in Figure 13, the performance of the cathode improves as the number of channel increases. Decreasing shoulder width, that is, increasing the number of channels, is equivalent to decreasing the length of a pipe in a fluid flow system which results in a higher pressure drop per unit length and a higher gas-flow rate. For the case in which the electrode thickness is

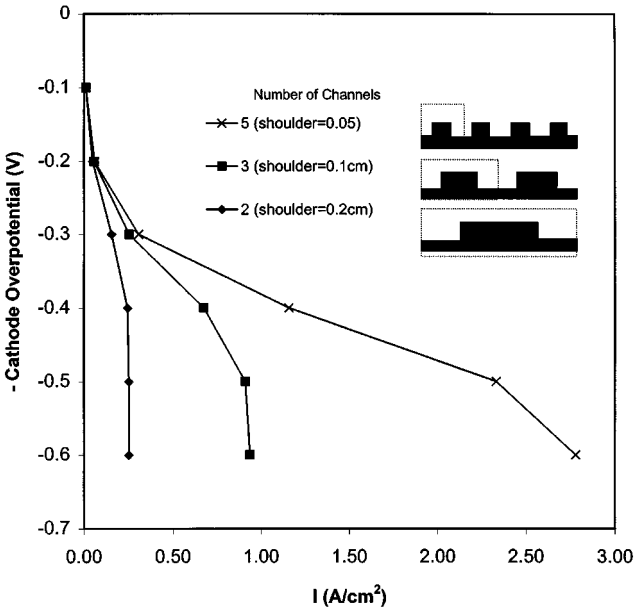

Figure 13. Effect of the number of channels on the performance of the cathode.

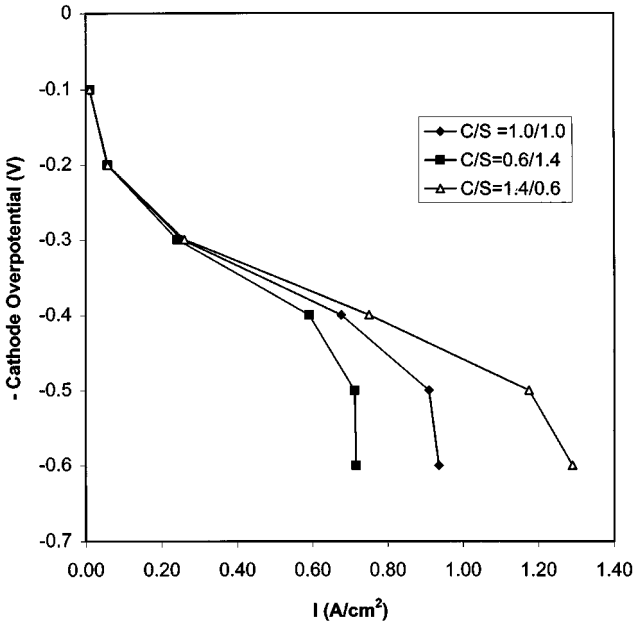

Figure 15. Effect of channel/shoulder ratio on the performance of the cathode.

kept the same and is within the optimal region, a higher gas-flow rate leads to both a thinner stagnant layer and higher reactant concentrations along the reaction interface and, consequently, higher current densities.

Both Figures 13 and 14 show that the number of channels has a very strong effect on the performance of the cathode operated under a fixed differential pressure. More channels are obviously preferred. However, the number of channels can be limited by the effect of gas bypassing as explained in the previous section and by the manufacturability and cost.

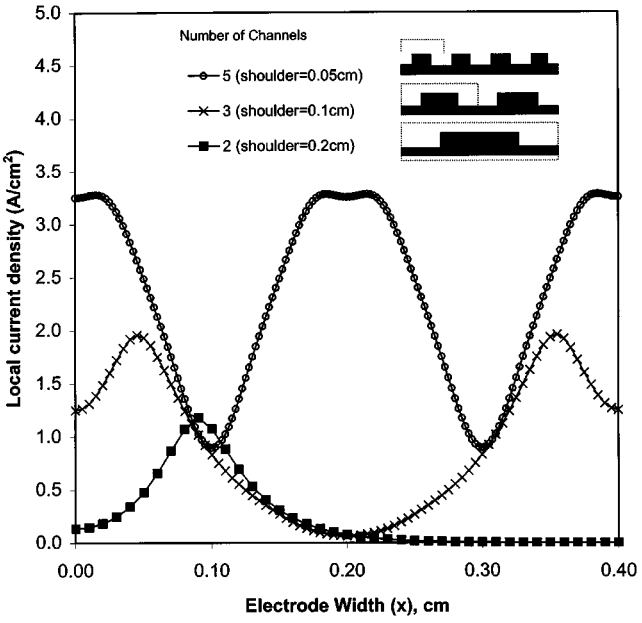

Figure 14. Effect of the number of channels on the current density profile along the electrode width (at an overpotential of 0.5 V).

Effect of the Ratio between the Channel and Shoulder Widths

In previous sections, the effects of the number of channels were investigated with the channel to shoulder width ratio held fixed at one. In this section, for a fixed width of electrode, the effects of the ratio between the channel and shoulder widths (C/S ratio) are investigated. The total width of the channels plus a shoulder and the electrode thickness are kept constant, and the ratio between the channel and shoulder widths is varied within one repeating unit, consisting of a half of the inlet channel, a shoulder, and a half of the outlet channel. Therefore, when the channel to shoulder ratio increases, the channel width increases and the shoulder width decreases. The results are presented in Figures 15 and 16, and can be explained as follows. As the channel width increases, the region of low y-direction velocity increases because most of the gas flows through the region close to the inlet/shoulder corner. This results in less oxygen flow to the region near the center of the inlet channel and higher back diffusion of water vapor toward the inlet with the net result being low oxygen concentration at the electrode reaction interface above most of the inlet region and low current densities. However, the gain in current density by higher gas-flow rate as the result of having a shorter shoulder width is more than the loss in current density in the region above the inlet by having larger inlet width. This is clearly illustrated by the local current profiles of the $C/S = 1/1$ and $C/S = 1.4/0.6$ given in Figure 16. On the other hand, when the channel width is reduced to make room for a larger shoulder width, the performance decreases. This decrease in performance is attributed to a lower gas-flow rate as the pressure gradient

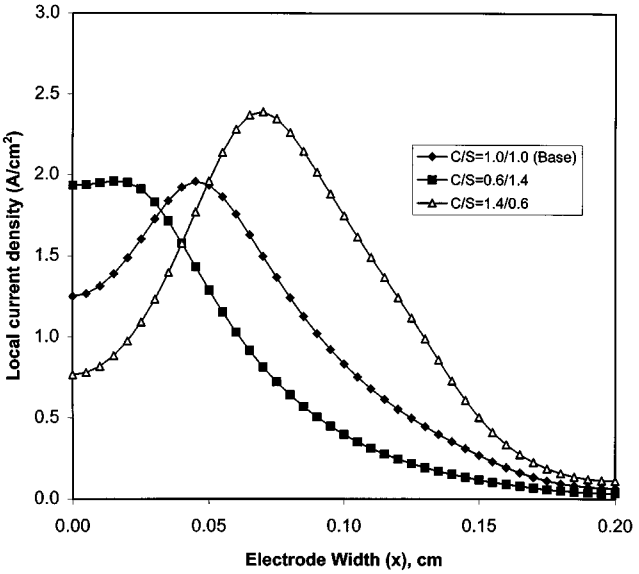

Figure 16. Effect of channel/shoulder ratio on the current density profile along the electrode width (at an overpotential of 0.5 V).

(pressure drop per unit length) is reduced when the channel width gets wider. Consequently, it is clearly shown here that to get higher performance, shorter shoulder width is preferred.

Now keep in mind that, the shoulders, which are the only parts in contact with the electrode, are needed for current collection. Lower contact area by having higher C/S ratio might result in higher cell ohmic resistance. Therefore, its dimension and the dimensions of the inlet and outlet channels must be considered together in the optimization of the PEM fuel cell performance.

Conclusions

A 2-D, two-phase, multicomponent transport model was developed to investigate the effects of the gas and liquid water hydrodynamics on the performance of an air cathode of a PEM fuel cell in contact with an interdigitated gas distributor. Darcy's law was used to describe the transport of the gas phase. The transport of liquid water through the porous electrode is driven by the shear force of gas flow and capillary force. A momentum equation that accounts for these driving forces was derived to describe the transport of the liquid phase in the porous electrode.

From the model results, the following conclusions are reached:

(1) Liquid water transport and evaporation are two main water removal mechanisms in a cathode in contact with an interdigitated flow field.

(2) A higher differential pressure between inlet and outlet channels will improve the electrode performance (that is, average current density) because of better oxygen transport and liquid water removal.

(3) The electrode thickness needs to be optimized to get optimal performance because a thinner electrode may reduce gas-flow rate and a thicker electrode may increase the diffusion layer thickness.

(4) For a fixed-size electrode, more channels and shorter shoulder widths are preferred.

Acknowledgments

This work was supported by the National Science Foundation under Grant No. CTS-9803364.

Notation

b = coefficient in Eq. 6a
C = mol concentration of gas, mol/cm^3
D_c = capillary diffusion coefficient of water, cm^2/s
D_i = diffusion coefficient of species i, cm^2/s
D_o^e = effective diffusion coefficient of oxygen in the electrode, cm^2/s
D_w^e = effective diffusion coefficient of water in the electrode, cm^2/s
F = Faraday constant, 96487 C/equivalent
h = electrode thickness, cm
I_{avg} = average current density, A/cm^2
L = electrode width, cm
$L1$ = half of inlet channel width, cm
$L2$ = half of outlet channel width, cm
R = gas constant, 82.06 cm^3·atm/mol·K or 8.314 J/mol·K
$\boldsymbol{\nu}$ = superficial velocity vector, cm/s
y = mass fraction
α = net water transfer coefficient per proton
η = overpotential for the oxygen reaction, V

Subscripts and superscripts

avg = average
c = cathode
g = gas
i = species
l = liquid
N = nitrogen
O = oxygen
r = reference state
x = direction across the channel and shoulder, cm
y = direction through the electrode, cm

Literature Cited

Adler, P. M., *Porous Media*: *Geometry and Transport*, Butterworth-Heinemann, Boston (1992).

Bear, J., and J. M. Buchlin, *Modeling and Applications of Transport Phenomena in Porous Media*, Kluwer Academic Publishers, Boston (1991).

Bernardi, D. M., and M. W. Verbrugge, "A Mathematical Model of the Solid-Polymer-Electrolyte Fuel Cell," *J. Electrochem. Soc.*, **139**, 2477 (1992).

Bird, R. B., W. E. Stewart, E. N. Lightfoot, *Transport Phenomena*, Wiley, New York (1960).

Cussler, E. L., *Diffusion*: *Mass Transport in Fluid Systems*, Cambridge University Press, New York (1984).

Gurau, V., H. Liu, and S. Kakac, "Two-Dimensional Model for Proton Exchange Membrane Fuel Cells," *AIChE J.*, **44**, 2410 (1998).

Kaviany, M., *Principles of Heat Transfer in Porous Media*, 2nd ed., Springer, New York, p. 467 (1995).

Nguyen, T. V., and R. E. White, "A Finite Difference Procedure for Solving Partial Differential Equations," *Comput. Chem. Eng.*, **11**, 543 (1987).

Nguyen, T. V., "A Gas Distributor Design for Proton-Exchange-Membrane Fuel Cells," *J. Electrochem. Soc.*, **143**, L105 (1996).

Nguyen, Trung Van, "Modeling Two-Phase Flow in the Porous Electrodes of Proton-Exchange-Membrane Fuel Cells Using the Interdigitated Flow Fields," *Proc. Vol. of Symp. on Tutorials in Electrochemical Engineering-Mathematical Modeling*, **PV 99-14**, The Electrochemical Society, Inc., Pennington, NJ, 222 (1999).

Nouel, K. M., and P. S. Fedkiw, ''Nafion-Based Composite Polymer Electrolyte Membranes,'' *Electrochimica Acta*, **43**, 2381 (1998).
Paik, Woon-kie, T. E. Springer, and S. Srinivasan, ''Kinetics of Fuel Cell Reactions at the Platinum/Solid Polymer Electrolyte Interface,'' *J. Electrochem. Soc*., **136**, 644 (1989).
Sone, Y., P. Ekdunge, and D. Simonsson, ''Proton Conductivity of Nafion 117 as Measured by a Four-Electrode AC Impedence Method,'' *J. Electrochem. Soc*., **143**, 1254 (1996).
Wang, C. Y. and P. Cheng, ''Multiphase Flow and Heat Transfer in Porous Media,'' *Advances in Heat Transfer*, **30**, 100 (1997).
Wang, J. T., and R. F. Savinell, ''Simulation Studies on the Fuel Electrode of a H2-O2 Polymer Electrolyte Fuel Cell, *Electrochimca Acta*, **37** 2737 (1992).
Watanabe, M., H. Uchida, and M. Emori, ''Analyses of Self-Humidification and Suppression of Gas Crossover in Pt-Dispersed Polymer Electrolyte Membranes for Fuel Cells,'' *J. Electrochem. Soc*., **45**, 1137 (1998).
West, A. C., and T. F. Fuller, ''Influence of Rib Spacing in Proton Exchange Membrane Electrode Assemblies,'' *J. of Appl. Electrochemistry*, **26**, 557 (1996).
Wood, David, III, Jung S. Yi, and Trung V. Nguyen, ''Effect of Direct Liquid Water Injection and Interdigitated Flow Field on the Performance of Proton Exchange Membrane Fuel Cells,'' *Electrochimica Acta*, **43**, 3795 (1998).
Yi, Jung S., and Trung V. Nguyen, ''The Effect of the Flow Distributor on the Performance of PEM Fuel Cells,'' *Proc. of First Int. Symp. on Proton Conducting Membrane Fuel Cells I*, **PV 95-23** Electrochem. Soc., 66 (1995).
Yi, J. S., and T. V. Nguyen, ''Hydrodynamics of Reactant Gas in the Electrode of PEM Fuel Cells with Inter-Digitated Flow Fields,'' *Electrochem. Soc. Meeting Extended Abstracts*, **96-2**, 974 (1996).
Yi, J. S., and T. V. Nguyen, ''Multi-Component Transport in Porous Electrodes in Proton Exchange Membrane Fuel Cells Using the Interdigitated Gas Distributors,'' *J. Electrochem. Soc*., **146**, 38 (1999).
Yi, Jung S., and Trung V. Nguyen, ''A Two-Phase Flow Model to Investigate the Hydrodynamics of Gas and Liquid Water in the Cathode of PEM Fuels Cells with Interdigitated Gas Distributors,'' Paper 107b, *AIChE Meeting*, Miami Beach, FL (Nov. 15–20, 1998).
Yi, Jung S., ''Characterization of Reactant Gases, Water and Heat Distributions in Proton-Exchange-Membrane Fuel Cells,'' PhD Diss. Univ. of Kansas, Lawrence, (1998).

Manuscript received Oct. 18, 1999, and revision received Mar. 24, 2000.